Amine functionalized nanodiamond promotes cellular adhesion, proliferation and neurite outgrowth

2014 Biomed. Mater. 9 045009

(http://iopscience.iop.org/1748-605X/9/4/045009)

IOP Publishing Biomedical Materials
Biomed. Mater. 9 (2014) 045009 (11pp) doi:10.1088/1748-6041/9/4/045009

Amine functionalized nanodiamond promotes cellular adhesion, proliferation and neurite outgrowth

A P Hopper[1], J M Dugan[1], A A Gill[1], O J L Fox[2], P W May[2], J W Haycock[1] and F Claeyssens[1]

[1] Department of Materials Science and Engineering, The University of Sheffield, Broad Lane, Sheffield, S3 7HQ, UK
[2] School of Chemistry, The University of Bristol, Bristol, BS8 1TS, UK

E-mail: f.claeyssens@sheffield.ac.uk

Received 5 March 2014, revised 15 May 2014
Accepted for publication 2 June 2014
Published 16 July 2014

Abstract
In this study, we report the production of amine functionalized nanodiamond. The amine functionalized nanodiamond forms a conformal monolayer on a negatively charged surface produced *via* plasma polymerization of acrylic acid. Nanodiamond terminated surfaces were studied as substrates for neuronal cell culture. NG108-15 neuroblastoma-glyoma hybrid cells were successfully cultured upon amine functionalized nanodiamond coated surfaces for between 1 and 7 d. Additionally, primary dorsal root ganglion (DRG) neurons and Schwann cells isolated from Wistar rats were also successfully cultured over a period of 21 d illustrating the potential of the coating for applications in the treatment of peripheral nerve injury.

Keywords: nanodiamond, Schwann cells, neurons, functionalization, amine, peripheral nerve

(Some figures may appear in colour only in the online journal)

1. Introduction

Diamond is known for its unique combination of properties including wear and corrosion resistance, hardness, low surface roughness, high refractive index and biocompatibility, which have been exploited for a wide range of applications [1–6]. Colloidal nanodiamond particles are prepared commercially through oxygen-deprived detonation of high explosives such as trinitrotoluene yielding particles of around 5 nm in diameter [7]. Nanodiamond has found applications in a wide range of areas as diverse as automotive lubricants, composite materials and drug delivery [4]. Recently, it has also been shown that surfaces coated with nanodiamond support the culture of neurons *in vitro*, highlighting its potential as a coating for medical devices that interface with the nervous system [1].

The development of effective neural interface materials for applications such as brain computer interfaces (BCIs) are required to better serve patients who suffer from either central or peripheral nerve injuries. To ensure success, these materials must exhibit low cytotoxicity and facilitate the action of neurotrophic factors while promoting cell proliferation and differentiation to the correct phenotype. It is therefore essential to develop a highly specialized and biomimetic surface in order to illicit the correct biological response. This may be achieved by modifying a substrate through the application of a bioactive coating or through chemical modification. In the case of nanodiamond, the material surface may be modified through treatments such as acidic oxidation [8] or reactive gas treatment [9], to achieve chemical homogeneity. Following surface modification, a wide range of bioconjugates or other molecules [2, 10–14] may be attached, promoting functionality whilst also retaining the original properties of the bulk nanodiamond material.

Our results indicate that nanodiamond particles that have been functionalized with an amine group, such as 10-amino-dec-1-ene, are beneficial for neural cell culture *in vitro* and are promising as a potential coating for neural implants *in vivo*. In this study, we use a short ultrasonic coating procedure to deposit a thin film of nanodiamond on the surface. The versatile nature of this deposition technique ensures that

even multi-faceted three-dimensional objects can be treated in a short period of time using readily available equipment. Although work has been conducted previously to assess the suitability of hydrogenated/oxygenated nanodiamond surfaces for neuronal cell adhesion and proliferation [1], the study of amine functionalized nanodiamond on neuronal cell lines has never before been carried out. It is anticipated that amine functionalized nanodiamond would mimic the local extracellular matrix (ECM) environment for neuronal culture in a manner similar to the use of poly-L-lysine (PLL [15]). This polypeptide is typically used to support neuronal culture on surfaces, but would not be suitable for implantation [16]. Viable alternatives to the use of PLL as a substrate coating for neuronal culture are therefore desirable.

2. Methods

2.1. Chemical methods

2.1.1. Synthesis of trifluoroacetic acid protected 10-aminodec-1-ene (TFAAD). All reagents were obtained from Sigma Aldrich (Gillingham, UK) unless otherwise stated. TFAAD was synthesized according to a method described elsewhere [17]. First, 10-undecenoyl chloride (50.0 g, 0.25 mol) was added to a sufficient quantity of tetrahexylammonium bromide (Acros Organics, Loughborough, UK, 0.6 mmol) in an ice bath. An aqueous solution of sodium azide (16.6 g in 50 ml) was then gradually added to the mixture within the ice bath and agitated using a magnetic stirrer. Once the reaction was complete, the organic fraction was separated, washed twice with an excess of distilled water, dried over anhydrous magnesium sulfate for 24 h and filtered. An excess of trifluoroacetic acid was then added to the acyl azide and the reaction mixture was heated to reflux under nitrogen for 6 h. The organic mixture was washed with a saturated solution of sodium bicarbonate, collected and subsequently dried over anhydrous magnesium sulfate for 24 h. The product was stored for later use at 4 °C.

2.1.2. Preparation of 10-amino dec-1-ene functionalized nanodiamond. Commercial detonation nanodiamond is usually supplied having undergone purification by acid wash. Nonetheless, such nanodiamond features a range of surface terminations that are uncharacterized and potentially variable. In order to ensure a uniform hydrogen-terminated surface, the detonation nanodiamond (Sigma Aldrich, Gillingham, UK) was hydrogenated by exposure to a hydrogen plasma flow for a total duration of 10 min prior to further functionalisation. Hydrogenation was carried out in 2 cycles of 5 min with microwave power of 0.8 kW and 500 sccm H_2 total gas flow, followed by 2 min in cold H_2 flow under a pressure of 100 Torr. The hydrogenated nanodiamond (h-ND) was then spread across a quartz slide, on top of which several drops of TFAAD were applied. A further quartz slide was positioned on top and fixed in place in preparation for irradiation with ultraviolet (UV) light. To determine the optimum UV irradiation time, a 6 W shortwave (254 nm) UV fluorescent lamp (model UVG-54, UVP, Upland, CA, USA) was positioned at a distance of 7.5 cm from the quartz slide. The material was irradiated up to a total of 120 h and samples were taken periodically for analysis by x-ray photoelectron spectroscopy (XPS). To prepare amine functionalized nanodiamond for use in further experiments, a more powerful UV lamp was employed (500 W Hg-Xe lamp, Hamamatsu Photonics, Welwyn Garden City, UK) at a distance of 20 cm from the quartz slide for a duration of 4 h to allow complete photochemical attachment to occur. The irradiance of the 6 W lamp at the distance used was 2.25 $mWcm^{-2}$, as quoted by the manufacturer, and the quoted irradiance of the 500 W lamp at 250 nm and at a distance of 20 cm was approximately 78 $mWcm^{-2}$. The effective dose from the 500 W lamp may therefore be considered equivalent to approximately 140 h of exposure to the lower power 6 W lamp. After UV irradiation, excess TFAAD was removed and the protected-amine-bound nanodiamond (tfaa-ND) was deprotected in acidified methanol (0.36 M HCl in methanol) at 65 °C over a period of 24 h to yield amine functionalized nanodiamond (am-ND) as evidenced by XPS.

2.1.3. Plasma polymerization. Glass coverslips were coated with an acrylic acid plasma polymer to provide a biocompatible anionic charged substrate in preparation for deposition of cationic amine functionalized nanodiamond (am-ND). Plasma polymerization was carried out using apparatus and reaction conditions that have been previously described [18]. Briefly, the reactor was composed of a cylindrical glass vessel (500 mm) with stainless steel end flanges and an external copper coil through which a 13.56 MHz radiofrequency generator was coupled inductively to the contents of the reactor. After loading the samples to be coated, the reactor was evacuated to a base pressure of 10^{-3} mbar. Acrylic acid vapor was introduced to a pressure of 2×10^{-2} mbar and the plasma was generated with a radiofrequency power of 10 W. Deposition was carried out for 10 min. Following the coating procedure, samples were used immediately for cell culture or further processing.

2.1.4. Ultrasonic deposition of amine functionalized nanodiamond. Glass cover slips coated with an acrylic acid plasma polymer were placed into polystyrene sample tubes with the coated surface facing upwards. An aqueous suspension of amine functionalized nanodiamond (am-ND, 5 mg/ml) was added dropwise until submerged. The tubes were placed in an ultrasonic bath for 15 min, after which samples were dipped in distilled water and dried in air. Samples were rinsed twice in phosphate buffered saline (PBS) prior to cell culture. This resulted in a surface of am-ND stabilized by the negatively charged acrylic acid terminated surface (AAND).

2.2. Materials analysis and microscopy

Surface chemistry was characterized by x-ray photoelectron spectroscopy (XPS). Spectra were recorded using a monochromatic Al Kα x-ray source (1486.6 eV) and an internal flood gun to reduce charging. Data were processed and analyzed using CasaXPS (version 2.3.12, Casa Software Ltd). High resolution spectra of the carbon 1s region were deconvoluted into constituent peaks using the fitting functionality of CasaXPS.

Peaks were fitted to a mixed model of 70% Gaussian and 30% Lorentzian composition. The full width at half-maximum of all component curves was set equal although the absolute value was not constrained.

10-amino-dec-1-ene functionalized nanodiamond (am-ND) was characterized by transmission electron microscopy (TEM). The nanodiamond was suspended in distilled water, with several drops of the resultant suspension applied to the surface of a copper TEM grid (diameter 3 mm, Agar Scientific, UK) and allowed to dry. Samples were analyzed using FEI Tecnai G2 Spirit and FEI Tecnai TF20 FEG transmission electron microscopes.

The surface topography of acrylic acid plasma polymer coated glass (AA) and amine functionalized nanodiamond coated samples was analyzed using a Veeco Instruments Nanoscope IV multimode atomic force microscope (AFM) in tapping mode. Micrographs were processed using WSXM software (Nanotec Electronica S.L., Spain).

2.3. Cell culture

Samples were sterilized for cell culture by incubation in 70% (v/v) ethanol for 1 h before rinsing three times in sterile PBS just prior to cell seeding. In cell culture experiments, three replicate samples were seeded with cells for each condition ($n = 3$) except for the viability assay (MTT) in which four replicate samples were used ($n = 4$).

2.3.1. NG108-15 neuroblastoma cells. NG108-15 neuroblastoma-glyoma hybrid cells were seeded upon glass, acrylic acid plasma polymer coated glass (AA) and amine functionalized nanodiamond treated acrylic acid coated glass (AAND) at a density of 1×10^5 cells/ml in Dulbecco's modified Eagle's medium (DMEM) supplemented with 2 mM glutamine, 100 U/ml penicillin, 100 μg/ml streptomycin and 0.25 μg/ml amphotericin B. The cells were cultured for 1, 2, 5 or 7 d at 37 °C and 5% CO_2 after which they were fixed for staining or assayed for viability.

2.3.2. Isolation and culture of primary Schwann cells. Primary Schwann cells and dorsal root ganglion (DRG) neurons were isolated from male Wistar rats using methods reported elsewhere [19]. Animals were sacrificed in compliance with the Animals (Scientific Procedures) Act 1986. Briefly, sciatic nerves were removed from male Wistar rats (2–3 months) and the connective tissue was subsequently discarded. The nerves were teased and cut into 2–3 mm segments and incubated with 0.05% (w/v) collagenase (Sigma, UK) at 37 °C for 1 h. This cell suspension was then filtered through a 40 μm Falcon filter (Becton Dickinson, USA) and centrifuged at 400 rcf for 5 min. The resultant cell pellet was washed with DMEM (including 10% (v/v) fetal calf serum) and resuspended in Schwann cell growth medium containing DMEM (PAA, UK), 2 mM glutamine, 10% (v/v) FCS, 1% (v/v) N2 supplement (Gibco BRL, UK), 20 μg/ml bovine pituitary extract, 5 μM forskolin (Sigma, UK), 100 U/ml penicillin, 100 μg/ml streptomycin and 0.25 μg/ml amphotericin B. The Schwann cell suspension was plated within 35 mm Petri dishes which had been previously coated with 0.5 mg poly-L-lysine/7 μg laminin (Sigma, UK). The cultures were maintained at 37 °C with 5% CO_2.

2.3.3. Isolation and dissociation of primary dorsal root ganglion (DRG) neurons. The spinal column was removed from male Wistar rats (two to three months) and divided along the sagittal plane exposing the dorsal root ganglia (DRGs). The DRGs were removed, trimmed and incubated (37 °C) within 2 ml F12 (Biosera, UK) (10% (v/v) collagenase IV) for 1 h. The medium was removed and a further 2 ml F12 media (10% (v/v) collagenase IV) was added for 45 min. This was also removed and the DRGs washed with fresh F12 media. The DRGs were then incubated (37 °C) in 2 ml F12 (10% (v/v) trypsin) for 30 min, after which 1 ml F12 (50% (v/v) foetal calf serum (FCS)) was added to arrest digestion. This solution was then removed and the DRGs were washed several times with F12 medium. The DRGs then underwent mechanical dissociation with the cell suspension being passed through a 70 μm filter. This suspension was centrifuged at 300 rcf for 5 min, after which all but 500 μl was removed; the remainder was used to resuspend the cell pellet, which was centrifuged at 500 rfc for 10 min. All unwanted cell debris was discarded with the neurons being resuspended in modified Bottenstein and Sato (BS) medium (50 ml medium: 0.005 g bovine serum albumin (BSA, Sigma, UK) and 500 μl N2 supplement (Gibco, UK) added to 49.5 ml F12 medium). Neurons were cultured upon AAND, glass and PLL surfaces, at first being allowed to adhere for 2 h before additional volumes of BS medium were added, supplemented with 77 ng/ml nerve growth factor (NGF).

2.4. Cell staining

2.4.1. Fluorescence staining of f-actin. After each time point, DMEM was removed from the NG108-15 cells which were washed once with phosphate buffered saline (PBS). To each well 500 μl of formalin (3.7% v/v) in PBS was then applied for 15 min after which the cells were washed twice with PBS. Staining was performed with fluorescein-conjugated phalloidin (Sigma, UK) to stain f-actin and DAPI (Sigma, UK) as a counterstain for 1 h and cells visualized *via* fluorescence microscopy (Axon Instruments).

2.4.2. Immunofluorescence staining. After 21 d culture, the media were removed from the dissociated DRGs or Schwann cell cultures which were then washed once with PBS. The cells were then fixed with formalin (3.7% v/v) for 15 min, washed with PBS, and permeabilised with 0.1% Triton X-100 (Sigma-Aldrich, Dorset, UK) for 20 min at 4 °C. Cells were washed again with PBS and then blocked with 3% (w/v) bovine serum albumin (BSA) for 60 min at 4 °C. This was followed by incubation with polyclonal rabbit anti-S100β (1:250) (Dako) and monoclonal mouse anti-βIII-tubulin (1:250 dilution, Lab Vision, UK) diluted in 1% (w/v) BSA overnight at 4 °C. The cells were washed twice with PBS to remove non-specific binding and incubated with Texas Red/FITC conjugated secondary anti-mouse/rabbit IgG antibody (1:100 in 1% (w/v) BSA) (Vector Labs, USA) for 90 min at room temperature.

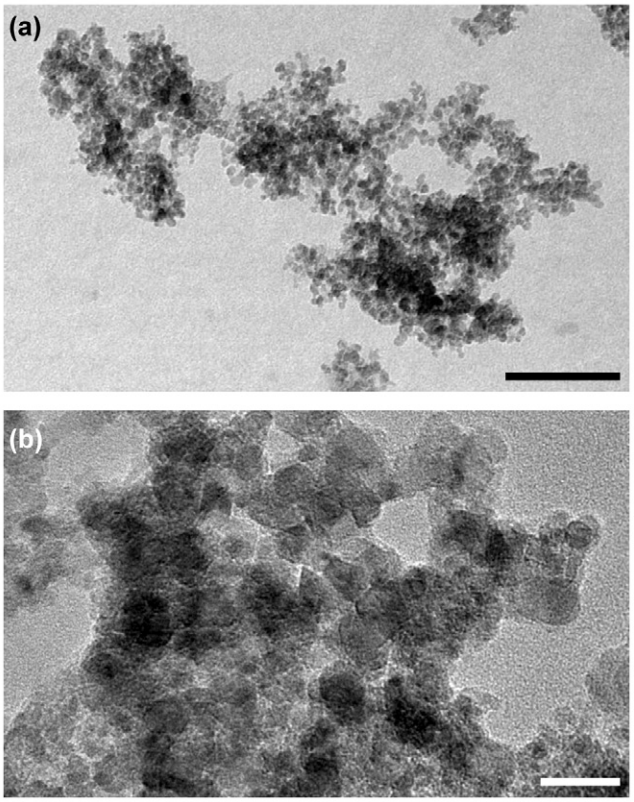

Figure 1. Transmission electron micrographs (TEM) of amine functionalized nanodiamond (am-ND). (*a*) 180 000 × magnification image of aggregated particles. Scale bar: 100 nm. (*b*) 345 000 × magnification image showing individual nanodiamond particles. Scale bar: 20 nm.

2.5. Cell viability assay

Cells were cultured at a density of 10 000 cells/ml within 24 well plates (Costar) over periods of 1, 2, 5 and 7 d. At each time point, the DMEM was removed from the wells to be analyzed, and the cells were washed once with PBS. MTT solution (thiazolyl blue tetrazolium bromide diluted to 0.5 mg/ml in PBS) was then added to each well of cells, and incubated at 37 °C and 5% CO_2 for 45 min. The MTT solution was then removed after which 300 μl acidified isopropanol (125 μl concentrated hydrochloric acid in 100 ml isopropanol) was added to each well and allowed to stand for 2 min. The resulting solution was transferred in triplicate 100 μl volumes to a 96 well plate and optical density was measured at an absorbance wavelength of 540 nm, referenced to 630 nm.

2.6. Statistical analysis

Statistical analysis of quantitative data (contact angle values, morphological image analysis and viability) was carried out using GraphPad Prism software (GraphPad Software, San Diego, USA). Single-factor analysis of variance (ANOVA) was carried out in order to determine the probability (p) of apparent differences between conditions arising solely from experimental variance. *Post hoc* comparison of means (Tukey method) was carried out in order to reveal specific differences between pairs of conditions. In the case of the morphological image analysis data, statistical analysis was carried out in order to compare conditions at each time point but comparisons between different time points were not made.

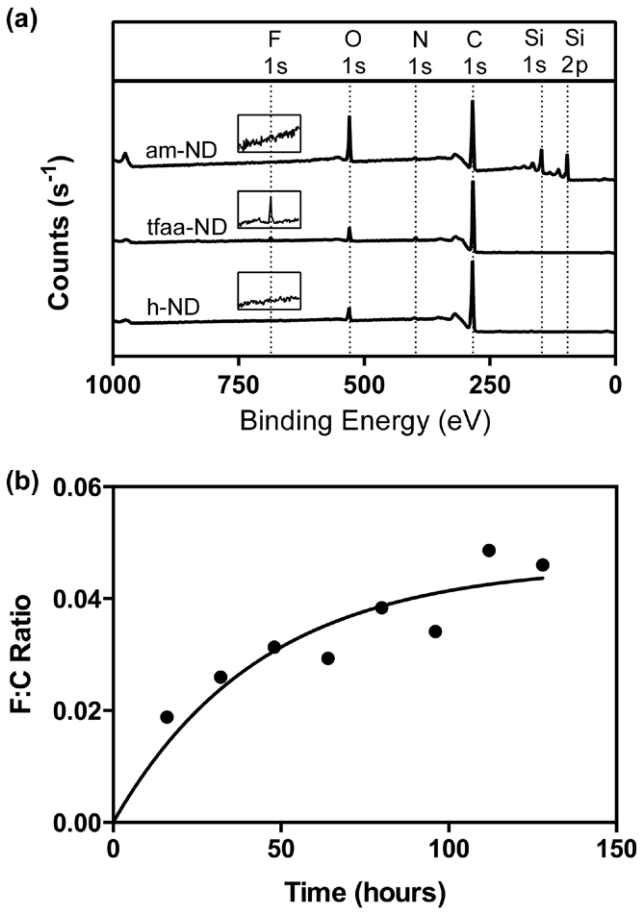

Figure 2. (*a*) Wideband x-ray photoelectron spectra (XPS) of hydrogenated nanodiamond (h-ND) and amine functionalized nanodiamond before (tfaa-ND) and after (am-ND) removal of the trifluoroacetyl protecting group. Labels show the element and orbital corresponding to each characteristic peak. The inset spectra show the fluorine 1s peak at 5 × y scale. (*b*) Plot of the ratio of integrated peak area of the fluorine 1s and carbon 1s peaks as a function of UV irradiation time. Curve shows a logarithmic decay as a guide to the eye.

3. Results

3.1. Characterization and functionalisation of nanodiamond

Amine functionalized nanodiamond (am-ND) was characterized by TEM which revealed aggregates of several hundred nanometers composed of individual particles (figure 1). Surface chemistry of the amine functionalized nanodiamond was characterized by XPS. Wideband spectra are shown in figure 2(*a*). As expected, the largest peak corresponded to electrons ejected from the C 1s orbital. Small peaks corresponding to Si 1s and 2p electrons were also present due to the underlying Si substrates used to support the ND materials during analysis. In addition, small peaks corresponding to O 1s and N 1s orbitals were observed in all three spectra. Some

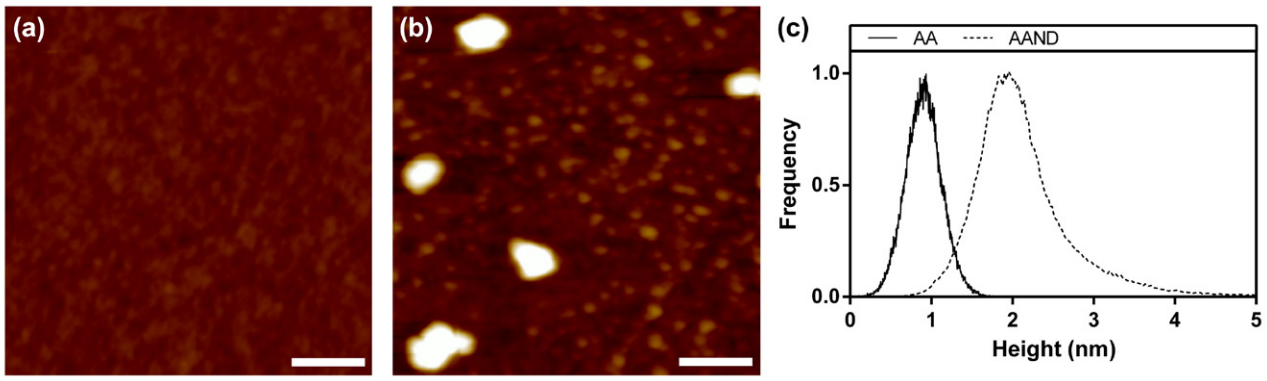

Figure 3. Atomic force microscopic (AFM) analysis of culture surfaces. (*a*) AFM topography image of acrylic acid plasma polymer coated glass (AA). (*b*) AFM topography image of amino functionalized nanodiamond deposited on acrylic acid plasma polymer coated glass (AAND); z-scale: 10 nm; scale bars: 100 nm. (*c*) Height distribution plots of the topography images. The root mean square roughness (Rq) of the AA and AAND surfaces was 0.22 nm and 1.5 nm, respectively.

oxygen may be present in the materials due to a small degree of surface oxidation and nitrogen should be present due to trifluoroacetamide or amine groups in the functionalized nanodiamond. Due to the high surface area of ND particle coated substrates, however, adsorption of N_2 and O_2 may also be expected. A small peak at high binding energy corresponding to F 1s electrons was clearly observed in the functionalized nanodiamond prior to deprotection but not in hydrogenated nanodiamond or deprotected amine functionalized nanodiamond. Due to the possible confounding effect of N_2 adsorption, an F 1s peak area relative to C 1s was used to quantify the relative degree of functionalization with increasing duration of UV exposure during photochemical functionalization (figure 2(*b*)). Fluorine content of the functionalized nanodiamond prior to deprotection clearly increased with time although the rate of functionalization decreased as the reaction proceeded.

3.2. Deposition and characterization of culture surfaces

Glass coverslips were coated with an acrylic acid plasma polymer (AA) and some were further treated with amine functionalized nanodiamond (AAND). The topography of the sample surfaces was analyzed using AFM (figure 3). AA surfaces appeared smooth and uniform with a small degree of nanoscale roughness (figure 3(*a*)). AAND surfaces, however, appeared completely coated with amine-functional nanodiamond particles and were considerably rougher than the AA surfaces (figure 3(*b*)). The majority of deposited particles appeared to be single particles of nanodiamond a few naometers in height. In addition, small aggregates of 8–10 nm in height were also deposited. AFM height distributions (of all measured datapoints) are shown in figure 3(*c*). The modal height for the AA and AAND surfaces were approximately 1 nm and 2 nm, respectively, with the distribution for AA being roughly symmetrical and the distribution for AAND being skewed toward values of greater height.

Surface chemistry of the samples was analyzed by XPS. High resolution scans of the C 1s peak are shown for AA in figure 4(*a*) and AAND in figure 4(*b*). In both cases, the C 1s peaks were asymmetrical due to multiple chemical states of carbon in the materials. Contributing components, corresponding to the major chemical states observed, were quantified by deconvolution and are shown as dashed curves in figures 4(*a*) and 4(*b*). Relative proportions, as percentage contributions to the C 1s peak, are given in table 1. A greater proportion of aliphatic carbon (or carbon with no bonds to heteroatoms) and carbon singly bonded to a more electronegative heteroatom (O or N) was observed in AAND samples compared to AA. Conversely, a lower proportion of carbon in carbonyl or carboxylic acid groups was observed in AAND compared to AA. As expected, therefore, relative contributions to the C 1s peak from carbonyl or carboxylic acid groups was lower for AAND as amine functionalized nanodiamond shielded the underlying plasma polymer during analysis. Increased aliphatic or pure carbon in the AAND samples is consistent with the presence of carbon-rich nanodiamond and the increased proportion of carbon singly bonded to O or N may indicate the presence of amine groups at the nanodiamond surface as a result of functionalization.

The hydrophobicity of the surfaces was assessed by water contact angle analysis using the sessile drop method (figure 4(*c*)). Contact angles on glass, AA and AAND surfaces were determined as 50° (±6°), 56° (±4°) and 67° (±7°), respectively. The AAND was slightly more hydrophobic than either the glass or AA surfaces although all surfaces may be considered relatively hydrophilic with contact angles less than 90°.

3.3. Culture of NG108-15 cell line

NG108-15 cells were cultured on glass (negative control), PLL (positive control), AA and AAND surfaces in serum-free differentiation medium. Cultures were fixed for microscopy and stained for f-actin after 1, 2, 5 and 7 d in culture. Fluorescence micrographs of NG108s after 7 d are shown in figure 5. Adhesion and growth were observed on all surfaces although fewer cells were observed on the glass negative control and the cells adopted a small, rounded morphology (figure 5(*a*)). In contrast, cells grown on PLL positive control surfaces were well spread and extended long neurite-like

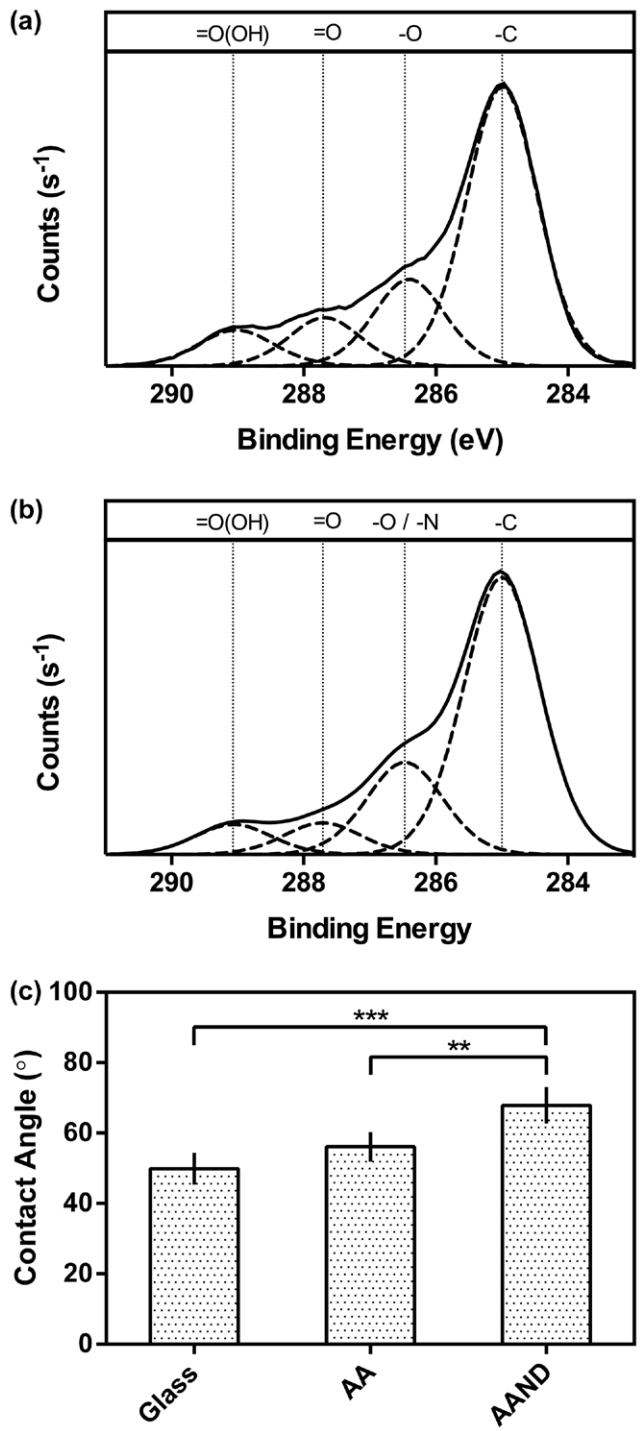

Figure 4. (*a*) Carbon 1s narrowband x-ray photoelectron spectrum (XPS) of acrylic acid plasma polymer coated glass (AA). (*b*) Carbon 1s narrowband XPS spectrum of amino functionalized nanodiamond deposited on acrylic acid plasma polymer coated glass (AAND). The asymmetric carbon 1s peaks were deconvoluted and the component curves are displayed with dashed lines. Indications of the likely chemical state corresponding to each component curve are given. (*c*) Water contact angle of glass, AA and AAND surfaces. The numerical values were 50° (±6°), 56° (±4°) and 67° (±7°), respectively. Statistical differences are displayed with braces; *** indicates a statistical difference with $p < 0.001$ and ** indicates a difference at $p < 0.01$.

Table 1. X-ray photoelectron spectroscopy of surfaces for cell culture. Glass samples coated with acrylic acid plasma polymer (AA), some of which were then also treated with amino-functional nanodiamond (AAND), were analysed by x-ray photoelectron spectroscopy (XPS). Percentages of contributing chemical environments of carbon were determined by deconvolution of carbon 1s peaks from high resolution spectra.

	–C (%)	–O/–N (%)	= O (%)	= O(OH) (%)
AA	61.7	19.2	10.7	8.4
AAND	64.3	21.4	7.3	7.0

processes (figure 5(*b*)). On AA the cells adhered and presumably proliferated to the greatest extent compared to the other surfaces (figure 5(*c*)). In comparison to the PLL positive control, however, few neurite-like processes were observed. On AAND surfaces, cells adhered and extended many long neurite-like processes in a manner very similar to that on the PLL positive control surfaces.

Automated image analysis of fluorescence micrographs was carried out in order to quantify morphological characteristics (figure 6). The percentage of cells bearing neurites is shown in figure 6(*a*). Few cells growing on glass or AA surfaces possessed neurites after 1 d in culture, in agreement with the micrographs shown in figure 5. By day 7, there was no increase in neurite bearing cells on glass or AA and no difference statistically between the two surfaces. In contrast, cells growing on PLL positive control surfaces and AAND surfaces frequently presented neuritic processes and the proportion of neurite bearing cells increased steadily over the 7 d in culture. By day 7, there was no statistical difference between PLL and AAND surfaces. A similar trend was observed in the average length of neurites (figure 6(*b*)). On glass, the length of neurites decreased over the 7 d in culture. Some increase in neurite length was observed on AA surfaces, although the length was always statistically lower than on AAND and PLL surfaces upon which a steady increase in neurite length was observed over the 7 d. By day 7, the average neurite length on the AAND surfaces was nearly as great as on PLL.

Viability of NG108s growing on the various surfaces was assessed by the MTT assay (figure 6(*c*)). Viability was statistically far greater on AA, AAND and PLL surfaces compared with the glass negative control. The greatest viability was observed on AA surfaces, likely indicating the largest cell population and rate of proliferation, although no statistical difference was observed on AA or AAND surfaces compared with the PLL positive control.

3.4. Culture of primary Schwann cells and dissociated dorsal root ganglion neurons

Primary rat Schwann cells were cultured on glass, AA, AAND and PLL surfaces. After 21 d in culture, the cells were fixed and stained for S100β, a marker of the Schwann cell phenotype. Fluorescence micrographs are shown in figure 7. On glass, the cells adhered and grew successfully, adopting a characteristic elongated morphology

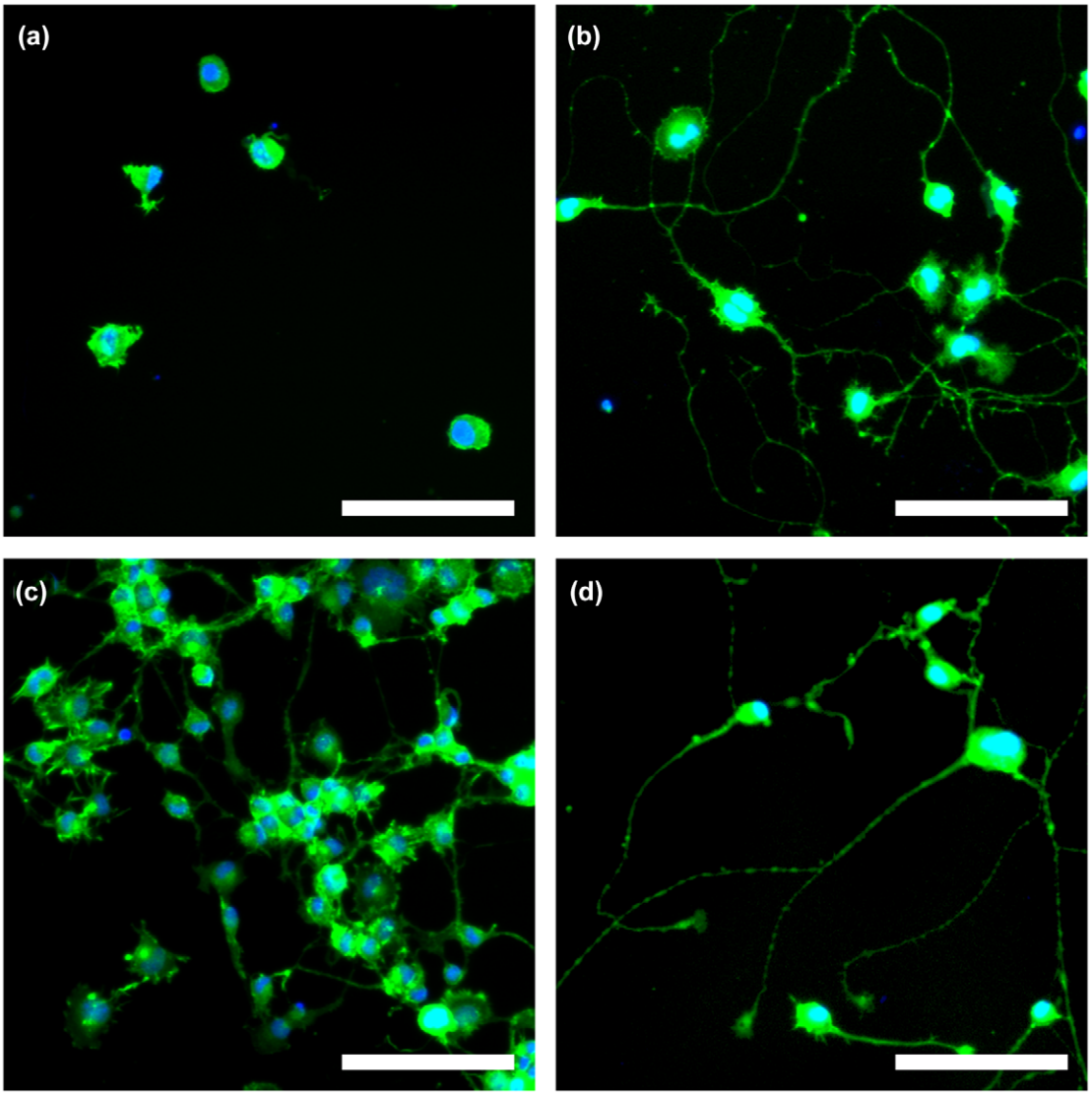

Figure 5. Fluorescence micrographs of NG108-15 cells fixed after 7 d in culture and stained for f-actin (green) and nuclei (blue). (*a*) Cells grown on glass. (*b*) Cells grown on poly-L-lysine coated glass (PLL). (*c*) Cells grown on acrylic acid plasma polymer coated glass (AA). (*d*) Cells grown on amine functionalized nanodiamond deposited on acrylic acid plasma polymer coated glass (AAND). Scale bars = 150 μm.

with extended processes in a bipolar or tripolar configuration (figure 7(*a*)). After 21 d in culture, however, the cells remained subconfluent on glass. In contrast, a dense confluent monolayer formed on PLL positive control surfaces, with the cells exhibiting the characteristic elongated bipolar morphology observed in confluent culture. On AA the cells remained subconfluent and did not present the characteristic morphology, instead adopting a polygonal cobblestone morphology (figure 7(*c*)). On AAND surfaces, the cells formed a confluent monolayer and exhibited a morphology indistinguishable from the PLL positive controls (figure 7(*d*)).

Dorsal root ganglia from adult rats were dissociated and the resulting single cells were seeded to glass, PLL and AAND surfaces and allowed to adhere and grow for 21 d. The cells were then fixed and stained for S100β as a marker for glia and βIII-tubulin as a neuronal marker. Fluorescence micrographs are shown in figure 8. No adhesion of glial or neuronal cells was observed on glass after 21 d, indicating that glass does not support mixed neuronal cultures under the conditions employed here (figure 8(*a*)). In contrast, extensive cell adhesion was observed on PLL positive control surfaces (figure 8(*b*)) and on AAND surfaces (figure 8(*c*)). No obvious difference was observed between PLL and AAND surfaces, each supporting adhesion of glial cells exhibiting an elongated bipolar morphology indicative of the Schwann cell phenotype interspersed with neuronal cells extending very long neuritic processes that were strongly positive for βIII-tubulin. It was apparent that the AAND surfaces supported culture of primary dorsal root ganglion neurons at least as well as PLL, the standard synthetic adhesion substrate employed in such culture methods.

4. Discussion

We have successfully functionalized hydrogenated nanodiamond particles using a well characterized photochemical method in which functional long-chain alkenes (such as TFAAD) are grafted to the diamond surface by irradiation with ultraviolet light [20]. It has been shown that, following photochemical attachment, amine molecules remain strongly bound to the diamond surface [21]. Indeed, AFM measurements illustrated that 100 nN of force from the AFM tip was required to strip a diamond surface of amine molecules. Interestingly, ultraviolet light (254 nm, 4.88 eV) is insufficient to cause bulk excitement of electrons across a 5.48 eV band gap at the diamond-alkene interface. The process by which TFAAD attachment occurs has therefore been speculated upon. Recently, a mechanism has been developed whereby electrons are photoemitted from the hydrogenated diamond surface into the surrounding liquid TFAAD, generating a reactive site at the interface. The trifluoroacetamide terminal group acts as an electron acceptor, thus enhancing the reactivity of the molecule, whereby the amine group attaches to a hydrogenated surface by island formation [22].

The functionalized nanodiamond was characterized by XPS. Although the adsorption of N_2 made direct detection of the amine groups difficult, the clear presence of fluorine in the functionalized nanodiamond prior to deprotection clearly indicated that the photochemical functionalization process was successful. Indeed the relative quantity of fluorine increased with UV irradiation time, tailing off with time as the free sites on the nanodiamond surface were depleted in a manner consistent with findings published elsewhere [23], indicating that there is a maximum dosage where the surface functionalisation is saturated.

A plasma polymerized acrylic acid coating was deposited on the glass substrates in order to provide an anionic substrate for amine functionalized nanodiamond deposition. Since the plasma polymerization was conducted under relatively low power (15 W) there was a comparatively high proportion of COOH/R groups present (approximately 12%) due to a low degree of monomer fragmentation during the plasma process. This compares to a presence of carboxylate groups of 11% for AA plasma polymers deposited at 50 W and 7% at 150 W as noted elsewhere [24]. Nonetheless, the degree of crosslinking was sufficient to ensure the stability of the coatings, as no delamination was observed during the cell culture experiments.

All of the surfaces tested were relatively hydrophilic, although the AAND surfaces were slightly more hydrophobic than the glass or AA surfaces, likely due to the relatively low polarity of the decylamine functionalization and due to the carbon rich nanodiamond. With respect to AA, it may reasonably be expected that the greater the carboxylate/carboxylic acid concentration the lower the water contact angle and the more hydrophilic the surface due to a higher incidence of hydrogen bonding with water molecules. Such moderately hydrophilic surfaces favor the retention of native protein

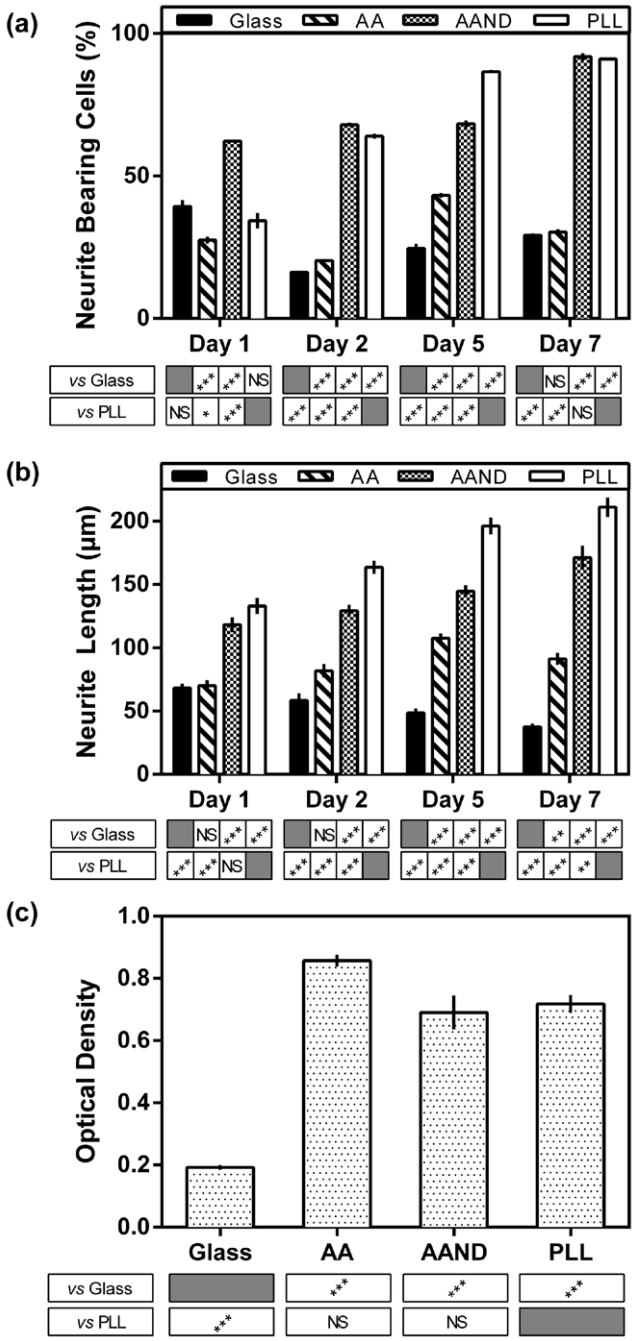

Figure 6. (*a*, *b*) Morphological image analysis from immunofluorescence micrographs of NG108-15 cells growing on different surfaces after 1 d, 2 d, 5 d and 7 d in culture. (*a*) Percentage of cells bearing neurites. (*b*) Average neurite length. Statistical differences between surfaces were determined at each time point by one-way analysis of variance (ANOVA) and Tukey's *post hoc* comparison of means. There were statistically significant differences between surfaces in both measurements at every time point with $p < 0.001$. Statistical differences vs the glass negative control and PLL positive control are displayed below each chart; *** and ** indicate a difference at $p < 0.001$ and $p < 0.01$, respectively; NS indicates no statistical difference ($p > 0.05$). (*c*) Viability assay (MTT) after culture of NG108-15 cells for 7 d on different surfaces. One-way ANOVA indicated a significant difference between surfaces at $p < 0.001$.

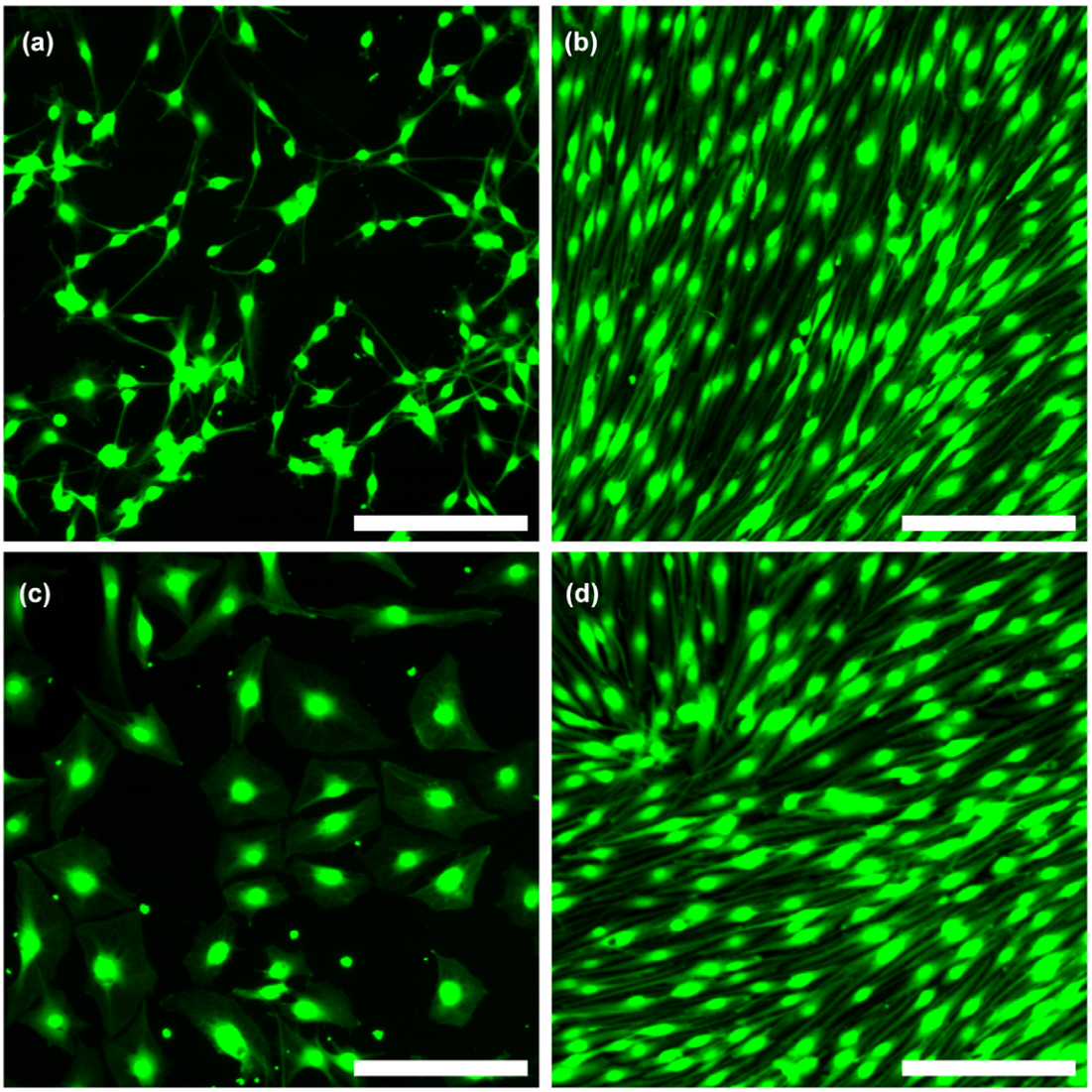

Figure 7. Fluorescence micrographs of primary rat Schwann cells fixed after 21 d in culture and stained for S100β (green). (*a*) Cells grown on glass. (*b*) Cells grown on poly-L-lysine coated glass (PLL). (*c*) Cells grown on acrylic acid plasma polymer coated glass (AA). (*d*) Cells grown on amine functionalized nanodiamond deposited on acrylic acid plasma polymer coated glass (AAND). Scale bars = 150 μm.

conformation, leading to favorable adherence conditions [25]. Although moderately hydrophilic surfaces are not a sole indicator of the ability of a surface to support cell growth, it has been widely discussed that they may be expected to encourage cell attachment and proliferation [26].

Both the AA surfaces and the AAND surfaces supported adhesion of NG108-15 cells. Furthermore, the AAND surfaces were comparable to the PLL positive control with respect to cell viability (or proliferation), the proportion of cells that extended neurites and the average length of neurites. Interestingly, a greater number of cells were observed growing on the AA surfaces than on the other surfaces studied, although fewer cells extended neurites and the average neurite length was shorter than on PLL and AAND surfaces. Given that the viability or proliferation was also greatest on the AA surfaces, it seems likely that this surface chemistry promotes NG108-15 proliferation with concomitant prevention or delay in terminal differentiation as evidenced in reduced neurite extension. Conversely, both of the amine bearing surfaces (PLL and AAND) appeared to promote terminal differentiation at the expense of proliferation in serum starved conditions. Indeed, although PLL and other synthetic cationic polypeptides such as polyornithine are widely used as growth matrices for neuronal culture, it has also been shown that amines presented as surface bound groups support and promote neuronal growth and differentiation in a similar fashion [27]. It has been suggested that amine groups may interact specifically with cells such as fibroblasts through membrane bound chondroitin sulfate proteoglycans (CSPGs [28]); whether this is the case for neuron-like cells such as the NG108-15 cell line is not certain. Nonetheless, it has also been suggested that CSPGs may play a crucial role in modulating neuronal differentiation *via* integrin mediated signaling [29]. Further work will be required, however, in order to properly elucidate the mechanism of interaction between synthetic amine bearing materials and neuronal cells.

In addition to the amine functionalized surface chemistry, the nanoscale topographical features presented by the

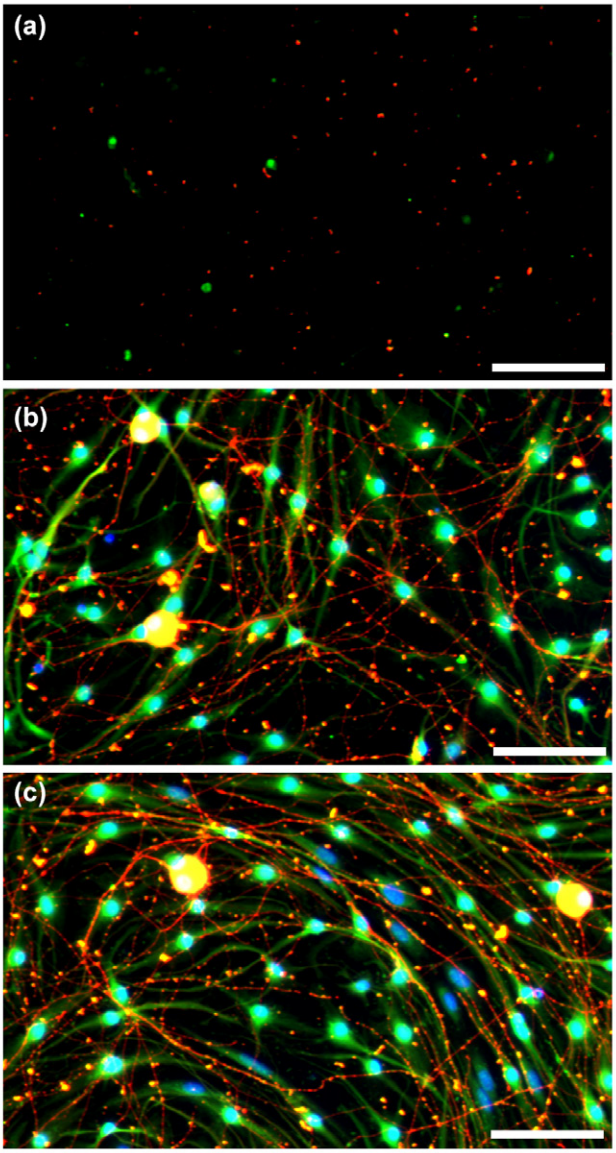

Figure 8. Fluorescence micrographs of dissociated dorsal root ganglia fixed after 21 d in culture and stained for S100β (green), βIII-tubulin (red) and nuclei (blue). (*a*) Cells grown on glass. (*b*) Cells grown on poly-L-lysine coated glass (PLL). (*c*) Cells grown on amine functionalized nanodiamond deposited on acrylic acid plasma polymer coated glass (AAND). Scale bars = 75 μm.

nanodiamond may also promote the adhesion and correct phenotype of neuronal cells. Non-functionalized nanodiamond has recently been shown to support neuronal cell culture using primary embryonic hippocampal neurons [1]. In addition to promoting neuronal adhesion, the nanodiamond surfaces also supported the formation of neuronal networks with functional synaptic connections. With the addition of amine functionalized surface chemistry, nanodiamond has the potential to provide an optimum surface for devices that interface with the central nervous system. Further to this, we have demonstrated for the first time that nanodiamond is highly promising for applications in peripheral nerve repair. Primary Schwann cells adhered and proliferated on the AAND surfaces, exhibiting the correct morphology and phenotype in a fashion indistinguishable from the PLL positive control surfaces. In contrast, on the AA surfaces the Schwann cells adopted an uncharacteristic polygonal morphology. Such morphological changes have been noted elsewhere and indicate a possible non-migratory Schwann cell phenotype [30, 31]. The potential for amine functionalized nanodiamond surfaces in peripheral nerve repair was also demonstrated here with the successful culture of dorsal root ganglion neurons. Again the AAND surfaces supported the adhesion of neurons with the correct phenotype in a fashion indistinguishable from the PLL positive control surfaces. We envisage that amine functional nanodiamond will be employed as a facile coating to be incorporated into devices that electronically connect with peripheral neurons (e.g. advanced prosthetics), and potentially in nerve guidance conduits in order to promote neuronal and glial regrowth and repair in response to peripheral nerve injury. Also given the recently demonstrated bactericidal properties of nanodiamond [32, 33], and the demonstration of ultrasensitive "in cell" temperature measurements, which could probe inflammation [34], we anticipate that this material has great potential in the development of new medical devices.

5. Conclusions

Hydrogenated nanodiamond particles were functionalized photochemically to yield an amine-terminated surface characterized by XPS. When electrostatically deposited on an acrylic acid plasma polymer substrate, the nanodiamond promoted neuronal cell adhesion, proliferation and neurite outgrowth. The nanodiamond also supported the growth of primary Schwann cells and dorsal root ganglion neurons with the correct phenotype over three weeks *in vitro*. Amine-functional nanodiamond provides a facile route for coating of medical devices which we anticipate will find applications in the treatment of peripheral nerve injury.

Acknowledgements

The authors are grateful to Dr Claire Hurley for assistance with XPS analysis, Dr Alex Walton and Dawn Bussey for assistance with AFM imaging, Chris Hill for assistance with TEM imaging and Prof John Haycock for the generous gift of primary Schwann cells and dorsal root ganglion neurons. Funding was provided by EPSRC.

References

[1] Thalhammer A *et al* 2010 The use of nanodiamond monolayer coatings to promote the formation of functional neuronal networks *Biomaterials* **31** 2097–104
[2] Huang H *et al* 2007 Active nanodiamond hydrogels for chemotherapeutic delivery *Nano Lett.* **7** 3305–14
[3] Lechleitner T *et al* 2008 The surface properties of nanocrystalline diamond and nanoparticulate diamond powder and their suitability as cell growth support surfaces *Biomaterials* **29** 4275–84
[4] Mochalin V N *et al* 2012 The properties and applications of nanodiamonds *Nat. Nano* **7** 11–23

[5] Krueger A *et al* 2008 Biotinylated nanodiamond: Simple and efficient functionalization of detonation diamond *Langmuir* **24** 4200–4
[6] Schrand A M *et al* 2007 Are diamond nanoparticles cytotoxic? *J. Phys. Chem.* B **111** 2–7
[7] Krueger A 2008 New carbon materials: biological applications of functionalized nanodiamond materials *Chem. Eur. J.* **14** 1382–90
[8] Martin R *et al* 2010 Fenton-treated functionalized diamond nanoparticles as gene delivery system *Acs Nano* **4** 65–74
[9] Spitsyn B V *et al* 2006 Inroad to modification of detonation nanodiamond *Diam. Relat. Mater.* **15** 296–9
[10] Chow E K *et al* 2011 Nanodiamond therapeutic delivery agents mediate enhanced chemoresistant tumor treatment *Sci. Transl. Med.* **3** 73ra21
[11] Zhang Q W *et al* 2011 Fluorescent plla-nanodiamond composites for bone tissue engineering *Biomaterials* **32** 87–94
[12] Tzeng Y K *et al* 2011 Superresolution imaging of albumin-conjugated fluorescent nanodiamonds in cells by stimulated emission depletion *Angew. Chem.-Int. Edn.* **50** 2262–5
[13] Shimkunas R A *et al* 2009 Nanodiamond-insulin complexes as pH-dependent protein delivery vehicles *Biomaterials* **30** 5720–8
[14] Martin R *et al* 2010 Nano-jewels in biology. Gold and platinum on diamond nanoparticles as antioxidant systems against cellular oxidative stress *Acs Nano* **4** 6957–65
[15] Young T H *et al* 2010 Surface modification of microporous pvdf membranes for neuron culture *J. Membrane Sci.* **350** 32–41
[16] Fischer D *et al* 2003 In vitro cytotoxicity testing of polycations: Influence of polymer structure on cell viability and hemolysis *Biomaterials* **24** 1121–31
[17] Sun B *et al* 2006 Covalent photochemical functionalization of amorphous carbon thin films for integrated real-time biosensing *Langmuir* **22** 9598–605
[18] Beck A J *et al* 2005 Plasma co-polymerisation of two strongly interacting monomers: acrylic acid and allylamine *Plasma Process. Polym.* **2** 641–9
[19] Kaewkhaw R *et al* 2012 Integrated culture and purification of rat Schwann cells from freshly isolated adult tissue *Nat. Protoc.* **7** 1996–2004
[20] Strother T *et al* 2002 Photochemical functionalization of diamond films *Langmuir* **18** 968–71
[21] Yang N *et al* 2008 Photochemical attachment of amine-layers on H-terminated undoped single crystalline CVD diamonds *Diamond Relat. Mater.* **17** 1376–9
[22] Wang X *et al* 2010 Photochemical grafting of alkenes onto carbon surfaces: Identifying the roles of electrons and holes *J. Phys. Chem.* C **114** 4067–74
[23] Colavita P E *et al* 2007 Photochemical grafting of n-alkenes onto carbon surfaces: the role of photoelectron ejection *J. Am. Chem. Soc.* **129** 13554–65
[24] Buttiglione M *et al* 2007 Behaviour of SH-SY5Y neuroblastoma cell line grown in different media and on different chemically modified substrates *Biomaterials* **28** 2932–45
[25] Colley H E *et al* 2009 Plasma polymer coatings to support mesenchymal stem cell adhesion, growth and differentiation on variable stiffness silicone elastomers *Plasma Process. Polym.* **6** 831–9
[26] Ayala R *et al* 2011 Engineering the cell-material interface for controlling stem cell adhesion, migration, and differentiation *Biomaterials* **32** 3700–11
[27] Wang J H *et al* 2010 Change in neuron aggregation and neurite fasciculation on eval membranes modified with different diamines *J. Biomed. Mater. Res. Part* A **94A** 489–98
[28] Massia S P and Hubbell J A 1992 Immobilized amines and basic-amino-acids as mimetic heparin-binding domains for cell-surface proteoglycan-mediated adhesion *J. Biol. Chem.* **267** 10133–41
[29] Gu W L *et al* 2009 Chondroitin sulfate proteoglycans regulate the growth, differentiation and migration of multipotent neural precursor cells through the integrin signaling pathway *BMC Neurosci.* **10** 15
[30] Koroleva A *et al* 2012 Two-photon polymerization-generated and micromolding-replicated 3D scaffolds for peripheral neural tissue engineering applications *Biofabrication* **4** 025005
[31] Weiner J A *et al* 2001 Regulation of schwann cell morphology and adhesion by receptor-mediated lysophosphatidic acid signaling *J. Neurosci.* **21** 7069–78
[32] Medina O *et al* 2012 Bactericide and bacterial anti-adhesive properties of the nanocrystalline diamond surface *Diamond Relat. Mater.* **22** 77–81
[33] Beranová J *et al* 2012 Antibacterial behavior of diamond nanoparticles against escherichia coli *Phys. Status Solidi* B **249** 2581–4
[34] Kucsko G *et al* 2013 Nanometre-scale thermometry in a living cell *Nature* **500** 54–U71